Received: 29 August 2019 | Revised: 15 June 2020 | Accepted: 14 July 2020

DOI: 10.1002/aic.16991

AIChE JOURNAL

THERMODYNAMICS AND MOLECULAR-SCALE PHENOMENA

An approach for predicting intracrystalline diffusivities and adsorption entropies in nanoporous crystalline materials

Mingbin Gao[1,2] | Hua Li[1] | Mao Ye[1] | Zhongmin Liu[1]

[1]National Engineering Laboratory for Methanol to Olefins, Dalian National Laboratory for Clean Energy, iChEM (Collaborative Innovation Center of Chemistry for Energy Materials), Dalian Institute of Chemical Physics, Chinese Academy of Sciences, Dalian, China

[2]University of Chinese Academy of Sciences, Beijing, China

Correspondence
Hua Li and Mao Ye, National Engineering Laboratory for Methanol to Olefins, Dalian National Laboratory for Clean Energy, iChEM (Collaborative Innovation Center of Chemistry for Energy Materials), Dalian Institute of Chemical Physics, Chinese Academy of Sciences, Dalian 116023, China.
Email: lihua@dicp.ac.cn (H. L.) and maoye@dicp.ac.cn (M. Y.)

Funding information
National Natural Science Foundation of China, Grant/Award Number: 91834302

Abstract

Confinement of molecules in nanoporous crystalline materials results in the unique and diverse characteristics of intracrystalline diffusion and adsorption, which can significantly affect the efficiency of gas separation and/or catalysis. However, understanding the interplay between confinement and intracrystalline diffusion and adsorption remains elusive at the quantitative level. In this work, it is found that the intracrystalline diffusion could be related to the hopping rate, which might be further connected to the translational and rotational motion of molecules and quantified by corresponding partition functions. Based on this analysis, the correlations capable of predicting the intracrystalline diffusivity and the adsorption entropy are developed. It is shown that the correlations can well capture the experimental and simulation results of more than 20 frameworks, including zeolites and MOFs, for a wide range of guest molecules. This approach can potentially serve as rapid screening tool for nanoporous crystalline materials in gas separation and catalysis.

KEYWORDS

adsorption, confinement, correlation, diffusion, nanoporous crystalline material

1 | INTRODUCTION

Diffusion and adsorption of guest molecules in nanoporous crystalline materials is at the heart of many industrial processes, in particular gas separation and heterogeneous catalysis.[1-5] In order to attain the enhanced yet tunable efficiency in gas separations and/or yield in catalytic reactions, it is becoming a common practice to take use of the confinement effect of nanoscale cavities and pores in sorbents and catalysts,[6-9] which are mostly nanoporous crystalline materials. For instance, the engineered nanoscale pores have been frequently applied in sorbents to control the behaviors of guest molecules and thus discriminate these molecules.[10] In addition, various experimental[11-13]and computational[14-18]studies have discovered that the shape selectivity of zeolite catalysts[18,19] is closely related to the diffusion of guest molecules in the nanoscale pores and cavities, which constraints the motion of large molecules and alter the selectivity of targeted products.

The understanding of interplay between confinement effect and molecular diffusion and adsorption, therefore, is of practical significance for the design, synthesis, and screening[20-22] of adsorbents and catalysts. A big challenge in this regard, however, is to quantify the diffusion and adsorption of guest molecules in the confined space of nanoscale. As shown in Figure 1a, the activation energy of diffusion of guest molecules in nanoporous crystalline materials is dependent upon the diameter of guest molecules and dimensions of the pores and cavities.[2,23] Larger molecules and/or smaller pores and cavities can increase energy barriers for molecular diffusion. Molecular dynamics (MD)[24-31] and atomistic simulations[32-34] are essentially used to predict and understand complex molecular diffusion as well as distribution of potential energy in nanoporous crystalline materials at different molecular loading and temperature. But the verification of force field in these simulations requires a large collection of experimental data and is time-consuming. Therefore, only very few studies focus on quantifying the effect of confinement on the intracrystalline diffusivity of guest molecules in nanoporous crystalline materials.[21,26,35-37] Rosenfeld[31] and Dzugutov[32] directly related the diffusivity of guest molecules to the excess entropy via a simple

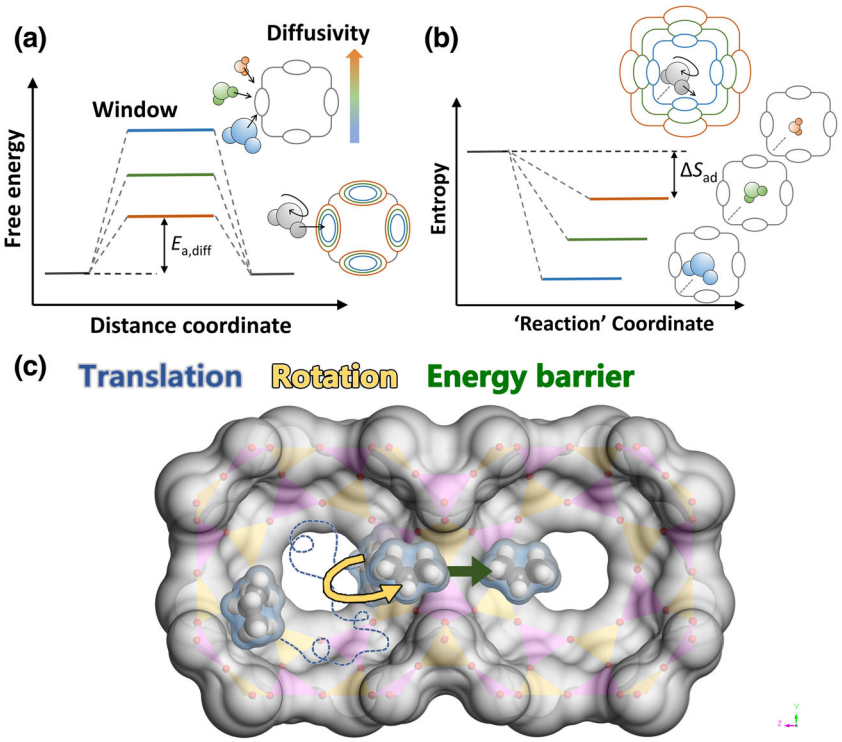

FIGURE 1 (a) Activation energy increase upon intracrystalline diffusion and (b) entropy loss upon adsorption in nanoconfined spaces, due to increased molecular diameter and/or decreased dimension of confined space. (c) The detailed processes of molecular intracrystalline diffusion proposed in this work. The molecular translation is affected by the fluctuation of pore wall, molecule needs to find suitable orientation by rotation to enter the window, and molecule needs to overcome the repulsive potential between molecule and window [Color figure can be viewed at wileyonlinelibrary.com]

exponential function. But the calculation of excess entropy is very difficult and time consuming.[38] In addition, the applicability of excess-entropy scaling to confining systems needs to be further verified. Sholl et al[21,35] developed a MD method to determine properties of diffusion for large scale of zeolites and MOFs materials and tested for small molecules as examples. Marbach et al[39] recently proposed a formalism to quantify the influence of fluctuation of wall structure on the diffusion of guest molecules. But it is a nontrivial task to relate the fluctuation of wall structure to real pores and cavities in nanoporous materials of interest.

Krishna[36] proposed that the degree of confinement, which is defined as the ratio of the characteristic diameter of molecules to that of the windows, can be regarded as an appropriate descriptor for confinement effect.[40,41] This descriptor, however, is shown only suitable for small molecules such as methane, neon, argon and xenon. An alternative approach is to connect the confinement effect to the adsorption entropy of adsorbed molecules in nanoporous crystalline materials, as shown in Figure 1b.[42-45] Moor et al[42,43,46] found that confinement has impact on the free degree of molecular translational and rotational motion of molecules by density functional theory (DFT) simulations. They found the carbon number of C_1-C_8 hydrocarbons is approximately a linear function of the adsorption entropy for FAU, BEA, MOR, MFI, and CHA zeolitic frameworks.[42,43,47] Dauenhauer et al[44] noticed that the lose of degrees of rotational freedom is sensitive to not only the types of molecules adsorbed but also the change of cavity volume in nanoporous material. Based on this, they proposed a simple correlation to predict the adsorption entropy based on the occupiable volume,[48] which can work well for C_3-C_9 hydrocarbons in nine zeolitic frameworks.[44] This motivates us to find a general approach to directly relate the adsorption entropy to the diameter of guest molecules and dimensions of confined spaces in different frameworks of nanoporous crystalline materials.

Actually Campbell et al[49] and Dauenhauer et al[44] found that the adsorption entropy could be related to the pre-factors in rate constants as well as desorption rate from the viewpoint of the transition state theory. Note that diffusion of guest molecules from one site to an adjacent site in nanoporous crystalline materials can be described by hops in the specified framework,[26,30] and the probability of molecules diffusing from one site to another site per unit time can be defined as hopping rate. On the one hand, the change of free energy along a "reaction coordinate" of diffusion,[30,50] together with the free energy of all possible molecular states in the pore and/or cavity, according to the transition theory, can be used to calculate the hopping rate.[30]On the other hand, the hopping rate can be interpreted as a result of combination of contributions by translational, rotational, electronic, vibrational and nuclear motion. Each contribution can be quantitatively described by the partition function of the corresponding motion. Therefore, it is the purpose of this work to establish a fundamental approach to quantify the intracrystalline diffusivity and adsorption entropy at infinite dilution based on the partition functions in confining systems. First, a theoretical analysis has been conducted for the diffusion of guest molecules in nanoporous crystalline materials by considering the effects of the translational and rotational partition functions, as well as the repulsive potential between the molecule and the wall of window, as shown in Figure 1c. Then the scaling relations, based on the theoretical analysis, have been established, which can efficiently predict intracrystalline diffusivity and adsorption entropy of a variety of molecules in a wide range of zeolites and metal organic frameworks (MOFs).

2 | THEORETICAL MODEL AND ANALYSIS

2.1 | Scaling relation between confinement and intracrystalline diffusion

The intracrystalline diffusion of guest molecules in nanoporous crystalline materials can be classified as self-diffusion and transport diffusion. At sufficiently low loading of guest molecules, that is, infinite dilution, the intracrystalline self-diffusivity and transport diffusivity can be considered equivalent.[51,52] Meantime, the intracrystalline diffusivity at infinite dilution can better characterize the interaction between the molecules and the wall of pores and/or cavities.[41] According to the transition state theory, the intracrystalline diffusivity of guest molecules can be estimated by[30,35]

$$D = n\lambda^2 k \tag{1}$$

where n is the dimension of the frameworks (n = 3, 1.5, and 1 for 1D, 2D, and 3D porous structures, respectively) of interest, λ the characteristic distance for a hop (m), which is approximated as the characteristic size of a cavity of framework,[30,35] and k the hopping rate (s^{-1}).[30,35] The hopping rate k can be interpreted as a result of total contribution of translational, rotational, electronic, vibrational and nuclear motions, which can be described by corresponding partition function (see Section 1 in Supporting Information). For the pure diffusion process of guest molecules without any chemical reactions occurring, it is reasonable to exclude the effects of vibrational (chemical bond) and nuclear contributions.[44] We follow the dynamically corrected transition state theory (dcTST)[26,29,30] that has been widely used in the simulations of molecular diffusion in confined media,[26,29,30] and assume the molecules on top of the barrier are in equilibrium. Further to that, as current work focused on the molecular diffusion at low loading, we can consider the Maxwell-Boltzmann distribution can be considered as a simple yet accurate representation of velocity distribution of molecules on the basis of kinetic gas theory of dilute gas.[27,53] Thus, the hopping rate in nanoporous crystalline materials is

$$k = \left(\frac{1}{\lambda}\sqrt{\frac{k_B T}{2\pi m}}\frac{f^*_{\text{trans.}}}{f_{\text{trans.}}}\frac{f^*_{\text{rot.}}}{f_{\text{rot.}}}\right)\exp\left(-\frac{E_{\text{a,diff}}}{RT}\right) \tag{2}$$

where k_B is the Boltzmann constant ($J\cdot K^{-1}$), m the molecular mass (kg), f^*/f the ratio of partition functions for molecules activated at the top of the barrier and that stayed in the cavity, $E_{\text{a,diff}}$ the activation energy of diffusion ($kJ\cdot mol^{-1}$), R the ideal gas constant ($J\cdot mol^{-1}\cdot K^{-1}$), and T the absolute temperature (K). Note that f^*/f is actually the probability of molecule entered the window over all molecules stay in the cavity by translation or rotation, and $E_{\text{a,diff}}$ represents the activation energy of diffusion required by a molecule to hop between adjacent lattice cavity. For simplicity, the ratio of translational partition function $f^*_{\text{trans.}}/f_{\text{trans.}}$ is defined as the factor $g_{\text{trans.}}$.

When molecules migrate to the window by translation, the change of the dimension of the confined spaces (i.e., change from cavity with large space to narrow window or vice versa) or pore constrictions[32,33] can enhance the frequency of collisions between molecules and wall[54] and lead to the decrease of diffusivity.[39] Marbach et al[39] showed that the diffusivity can be related to the fluctuations of nanopores by including the effect of structural constrictions:

$$g_{\text{trans.}j} = 1 - \frac{d^2_{\text{cage},j} - d^2_{\text{window},j}}{d^2_{\text{cage},j}} \tag{3}$$

where d_{cage} is the size of cavity, and d_{pore} is the window diameter (nm). The window diameter of nanoporous crystalline materials can be assumed to be uniform. Equation (3) implies that the large difference of dimension between cavity and window, or small cavity can have negative effect on diffusion.

Before molecules enter the small window of host materials, if the diameter of guest molecules is comparable to the dimension of the window, molecules need to adjust in particular rotation to get the suitable orientation in order to enter the window. In this sense, the rotational partition function, rather than the translational partition function, would dominate the pre-exponential factor of hoping rate. The shape of molecule is an important aspect for rotation of molecule passing through window. We assumed that a molecule can be modeled as an ellipsoid.[8,55] An shown in Figure S1, an ellipsoid is defined by its three axes, a, b, and c, where the length of three axes follows the order $a \le c \le b$. The structures of molecules were optimized by ωB97XD hybrid density function with 6-31G(d,p) basis sets by use of the Gaussian 09 package.[56] Thus, three axes of the ellipsoid can be measured based on the optimized molecular structures and corrected to van der Waals (vdW) radius of corresponding atom (e.g., H, C, O, and N). The molecular volume is assumed approximately equal to vdW volume V_{vdW}, which can be determined by critical temperature and pressure of fluid.[57,58] For the molecules with ellipsoidal approximation, the vdW volume satisfies $V_{\text{vdW}} = 2/3\cdot\pi\cdot(abc)$. It can be reduced to $V_{\text{vdW}} = 2/3\cdot\pi\cdot(\sigma_{\text{vdW}})^3$ for spherical molecules,[58] where the average diameter σ (= a = b = c) of molecule is assumed to vdW diameter. The detailed parameters for molecules studied in this work are listed in Table S2.

Based on Equation (S14), the formula $f^*_{\text{rot.}}/f_{\text{rot.}}$ of molecules i in framework j of nanoporous crystalline materials can be estimated by

$$\left(\frac{f^*_{\text{rot.}}}{f_{\text{rot.}}}\right)_{i,j} = \text{erf}\left(A\frac{d^p_{\text{window},j}}{\sqrt{\left(b_i^2+c_i^2\right)^q}}\right)\text{erf}\left(A\frac{d^p_{\text{window},j}}{\sqrt{\left(a_i^2+c_i^2\right)^q}}\right)\text{erf}\left(A\frac{d^p_{\text{window},j}}{\sqrt{\left(a_i^2+b_i^2\right)^q}}\right) \tag{4}$$

In Equation (4), each term respectively reflects the imposed limitation on rotation of molecules around axis a, b or c when they pass the window of host materials. Specifically, for the linear molecule (e.g., H_2, O_2, N_2, CO, and CO_2), it is known that a = c and the rotational partition function for b axis is 1, and thus the formula of $f^*_{\text{rot.}}/f_{\text{rot.}}$ becomes

$$\left(\frac{f^{*}_{\text{rot.}}}{f_{\text{rot.}}}\right)_{i,j} = \text{erf}\left(A\frac{d^{p}_{\text{window},j}}{\sqrt{\left(a_i^2+b_i^2\right)^{q}}}\right)\text{erf}\left(A\frac{d^{p}_{\text{window},j}}{\sqrt{\left(a_i^2+b_i^2\right)^{q}}}\right) \quad (5)$$

where A ($\text{nm}^{[q-p]}$), p and q are the fitting constants. The rotational partition function reflects that the possibility of molecules passing through the window. In Equation (4), therefore, each term respectively reflects the extent of limitation of rotation around axis a, b, or c imposed by the window. For instance, when molecule approaches the window, the extent of rotation of ellipsoidal molecule around axis c depends on the projected area of the a–b plane (Figure S1) and window diameter. In Equation (4), when the ratio of window diameter to $\sqrt{\left(a_i^2+b_i^2\right)}$ is sufficiently large, $f^{*}_{\text{rot.}}/f_{\text{rot.}}$ approaches 1, meaning molecule can pass through this window at any orientations. In contrast, if the ratio of window diameter to $\sqrt{\left(a_i^2+b_i^2\right)}$ decreases, $f^{*}_{\text{rot.}}/f_{\text{rot.}}$ may essentially reduce.

After molecules find suitable orientations and enter the window, the potential energy between molecules and window can significantly affect the translational velocity. The activation energy of diffusion $E_{\text{a,diff}}$ in confined spaces can be calculated by the repulsive potential. The Born–Mayer exponential term was only used to represent the energy barrier (repulsive potential) between molecules and windows of nanoporous crystalline materials, and the usual Lennard-Jones (L-J) potential was otherwise employed. The form of repulsive potential can be represented as $U^{\text{rep}}(r) = \varepsilon\cdot\exp(-Br)$ by Born–Mayer form,[59] where U^{rep} is the repulsive potential, r the distance between the molecule and window, and ε the potential well. The activation energy of diffusion can be written as $E_{\text{a,diff}} = C\cdot\exp(-Br)$ if the repulsive potential is considered as the predominant interaction. The distance r between the molecule of interest and the wall of window can be related to the average molecular diameter σ of the molecule by $r \sim -\sigma$. Therefore, the activation energy of diffusion can be approximated by

$$(E_{\text{a,diff}})_{i,j} = C_{\text{E},j}\exp\left(B_j\sigma_j\right) \quad (6)$$

where $C_{\text{E},j}$ is the constant of specific framework j ($\text{kJ}\cdot\text{mol}^{-1}$), and B_j the characteristic factor of the activation energy of diffusion in framework j (nm^{-1}). In Equation (6), for instance, the activation energy of diffusion of *n*-butane is higher than that of propane in ZIF-8 MOFs.[26] Note that *n*-butane has similar *a*- and *c*-axes as propane but much longer *b*-axis than that of propane. Here, for simplicity, the average molecular diameter (i.e., van der Waals diameter) was used to correlate the activation energy of diffusion.

To further identify the leading mechanism (i.e., the confinement and adsorption strength) affecting the intracrystalline diffusion, we carried out analysis based on density functional theory (DFT) calculations (see Section 2 in Supporting Information). The intracrystalline diffusivity Đ(0) at infinite dilution in SAPO-34 zeolites for three groups of molecules, that is, N_2 and CO, C_2H_6 and CH_3OH, and *iso*-C_4H_8 and *n*-C_3H_7OH, was summarized in Table 1. In each group, the two molecules have close molecular diameter but with different adsorption potential energy U_{ads}. As can be seen, the increased adsorption potential energy can slightly decrease the diffusivity, but the molecular diameter plays a more significant role in determining diffusivity.[60] To make further verification, Đ(0) of two groups of molecules in silicalite[61] (one is CH_4 and Ar, and the other is CF_4 and Xe) were compared. Each group of molecules have different L-J potential well but similar characteristic molecular diameter. As expected, Đ(0) of each group is almost identical and independent of L-J potential well. At this point, the major factor affecting intracrystalline diffusion might be contributed to the confinement. Therefore, it can be argued that the parameter B_j in Equation (5) are closely related to the structure of frameworks.

For the characterization of structure of zeolites and MOFs materials, the maximum included sphere diameter (MISD) and maximum free sphere diameter (MFSD)[48,62] will be used to describe the cavity size d_{cage} and window diameter d_{window}, respectively.[44] The establishments of MISD and MFSD have taken account of the interaction potential in frameworks.

2.2 | Scaling relation between confinement and adsorption entropy

Inspired by Equation (2), the pre-exponential factor of hoping rate can be interpreted as the entropic contribution in the form of $\exp(\Delta S^{\text{TS}}/R)$, where ΔS^{TS} is the entropy change associated with the molecules approaching the top barrier of diffusion as it stays in the cavity.[49] It can be identified that the loss of adsorption entropy is directly related to the characteristic diameter of molecules. Meanwhile, for molecules confined in the smaller cavities, the loss of degree of freedom will become more pronounced. Therefore, the dimension of cavity determines the loss of adsorption entropy. Assuming the parameter A_j^{ads} is approximately the negative of the dimension of cavity of the frameworks, we obtain

$$(-\Delta S_{\text{ads}}/R)_{i,j} = A_j^{\text{ads}}\sigma_i + C_{\text{A},j} \quad (7)$$

where ΔS_{ads} is the loss of the adsorption entropy ($\Delta S_{\text{ads}} < 0$) due to restricted motion of molecules in the confined cavities ($\text{J}\cdot\text{mol}^{-1}\cdot\text{K}^{-1}$), A_j^{ads} the correction factor for the framework j (nm^{-1}), which can

TABLE 1 The potential energy of adsorbed molecule and their corresponding intracrystalline diffusivity at infinite dilution in SAPO-34 zeolites at 300 K

Molecule	σ (nm)	U_{ads} (kJ/Mol)	Đ(0) (m^2/s)
N_2	0.313	−30.52	4.52×10^{-10}
CO	0.324	−113.27	2.09×10^{-10}
C_2H_6	0.372	−35.27	1.69×10^{-12}
CH_3OH	0.374	−103.90	7.05×10^{-13}
n-C_3H_7OH	0.441	−134.4	1.41×10^{-17}
iso-C_4H_8	0.442	−98.25	1.03×10^{-17}

reflect the effect of framework on adsorption entropy, and $C_{A,j}$ a constant (dimensionless).

3 | EXPERIMENTAL AND SIMULATIONS

3.1 | Measurements of diffusivity and adsorption isotherms

The synthesis of the SAPO-34 and DNL-6 zeolites has been reported in our previous work.[63,64] By use of the Intelligent Gravimetric Analyzer (IGA-100, Hiden Analytical), the uptake rate of methanol, propylene, propane, *n*-butene and *iso*-butene in SAPO-34 and DNL-*6* were measured. The intracrystalline diffusivity and surface permeability were decoupled as described in our previous work.[63] The detailed results and analysis of surface barrier and intracrystalline diffusion can refer to Section 1 in Supporting Information. Adsorption isotherms of ethylene, propane, *n*-butene and *iso*-butene were obtained using IGA techniques. Langmuir adsorption model was used to determine the adsorption enthalpy and entropy. For the detailed results and analysis refer to Section 2 in Supporting Information. By use of membrane permeation, the method of decoupling surface barrier and intracrystalline diffusion are introduced in Section 1 in Supporting Information.

3.2 | Molecular dynamics

MD simulations of self-diffusion behaviors of methane, ethane, propane and *n*-butane at low molecular loading inside zeolites were performed. The molecular loading was ~0.3 molecules/cage or channel of zeolites. The initial framework structures of FAU, EUO, LTA, and LEV were taken from the International Zeolite Associations database.[65] The selected super cells are $2 \times 1 \times 1$, $2 \times 1 \times 2$, $2 \times 1 \times 1$, and $2 \times 2 \times 1$ (in *x*-, *y*-, and *z*-directions) for FAU, EUO, LTA, and LEV, respectively. Periodic boundary conditions were applied in all three directions. The interatomic interactions were described by the condensed-phase-optimized molecular potentials for atomistic simulation studies (COMPASS) force field. The initial adsorption structures of molecules in zeolitic structures with fixed loading were obtained via Monte Carlo (MC) simulations in the NVT ensemble, where the particles number (N), volume (V), and temperature (T) are constant, based on the Metropolis method.[54] To ensure that the system is sampled under an equilibrated state, a minimum of 1×10^5 MC steps in the NVT ensemble are implemented. Each simulation was first conducted for 1 ns to reach equilibrium, and then continued for 5 ns to study the molecular diffusion. In the simulations, a specified temperature (i.e., 250, 300, and 350 K) was set and controlled by a Nosé thermostat.[27] The velocity Verlet algorithm was used to integrate the Newton's equations of motion with a time step of 1 fs. A cutoff radius of 18.5 Å was assumed for Lennard-Jones interaction potential calculation in all three directions. The Ewald & Group summation method with an Ewald accuracy of 10^{-5} kcal/mol was used for calculating electrostatic potential energy. The trajectories were recorded at time interval of 50 fs. All simulations in this work were carried out using the Materials Studio simulation package (Accelrys Software).

3.3 | Density functional theory (DFT) calculations

The adsorption entropy of diverse molecules in FAU, LTA, RHO and CHA zeolitic frameworks were obtained by DFT calculations.[56,66] The detailed structures, method and results could refer to Section 1 in Supporting Information.

4 | RESULTS AND DISCUSSIONS

4.1 | The correlation for intracrystalline diffusivities

To determine the parameters in Equations (4) and (6), the intracrystalline diffusivity Đ(0) of various molecules in FAU (this work), ZSM-5,[67] ZIF-8 MOF,[26] and SAPO-34[55,68-70] (this work) at 300 K were collected (see Section 1 in Supporting Information). Figure 2a shows $f^*_{rot.}/f_{rot.}$ as function of the ratio between molecular diameter and MFSD in FAU, ZSM-5, ZIF-8 MOF, and SAPO-34. Based on Equation (4), for the same framework, $f^*_{rot.}/f_{rot.}$ shows a remarkable decrease as $(abc)/d^3_{window}$ increases. This reflects that molecules can only enter the window with well suitable orientations when molecular diameter become sufficiently larger or the dimension of window becomes extremely small. Based on Equation (4), we obtain the parameters $A = 2.25 \pm 0.22$ (nm^{-2}), $p = 3$ and $q = 1$ by fitting the data as shown in Figure 2a.

In order to further illustrate the role of rotational partition function as discussed above, we have conducted a set of molecular dynamics (MD) simulations. We first determined the critical $f^*_{rot.}/f_{rot.}$ of propene for different scenarios. It is calculated that the critical $f^*_{rot.}/f_{rot.}$ of propene is 1.00 if rotation is completely free, 3.87×10^{-2} if rotation around one axis (for instance *a*-axis) is limited, 1.40×10^{-3} if rotations around two axes (for instance, both *a* and *c*-axes) are limited, and 1.20×10^{-4} if rotation around all three axes are limited. We then conducted the simulations on $f^*_{rot.}/f_{rot.}$ for propene molecules when approaching the windows of FAU. EUO, LTA, and LEV frameworks, as shown in Figure 3. It can be seen that, as a propene molecule passes through the 12-member ring of FAU framework, the $f^*_{rot.}/f_{rot.}$ obtained via Equation (4) is about 8.87×10^{-1}, which is close to 1.0 and indicates that the propene molecule can rotate in all three-dimension with minor limitation. When the propene molecule passes through the 10-member ring of EUO framework, $f^*_{rot.}/f_{rot.}$ reduces to 6.55×10^{-2} that is close to the critical $f^*_{rot.}/f_{rot.}$ of 3.87×10^{-2}, which demonstrates that the rotation around *a*-axis is severely limited. When the propene molecule passes through the 8-member ring of LTA framework, $f^*_{rot.}/f_{rot.}$ reduces to 9.57×10^{-3}, which, however, is a bit larger than the critical $f^*_{rot.}/f_{rot.}$ of 1.40×10^{-3}. A careful observation suggests that, in this case, the rotation of propene molecule

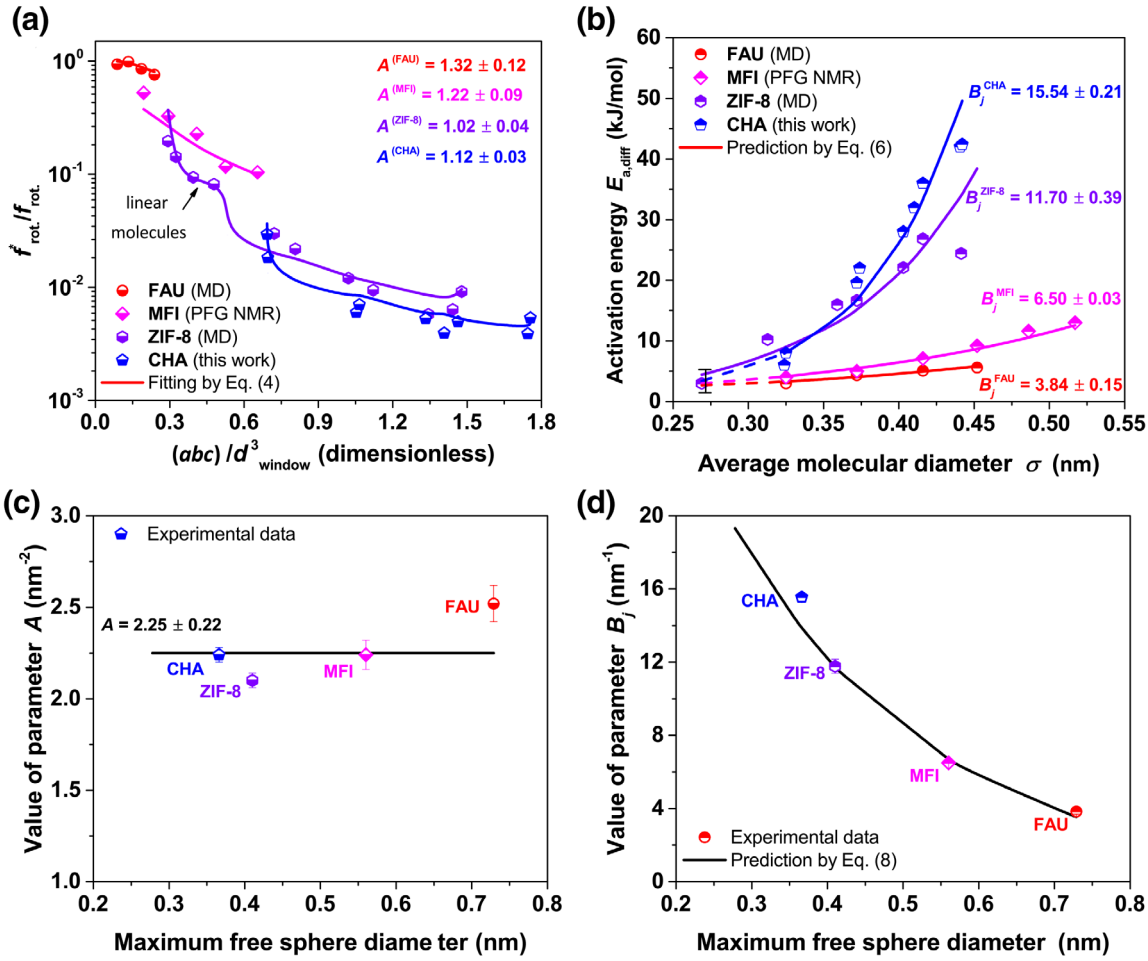

FIGURE 2 (a) $f^*_{rot.}/f_{rot.}$ as the function of the ratio between molecular diameter and MFSD in the FAU, MFI, ZIF-8 MOF and CHA, exponential fits by Equation (4). (b) Diffusion activation energy $E_{a,diff}$ as function of the average molecular diameter in the FAU, MFI, ZIF-8 MOF and CHA, exponential fits by Equation (6). (c) Parameter A_j as function of MFSD of framework, solid line represents linear fit by Equation (8). (d) Parameter B_j as function of MFSD of framework, solid line represents exponential fit by Equation (8) [Color figure can be viewed at wileyonlinelibrary.com]

around *a*-axis is limited while the rotation around *c*-axis is partially constrained when passing through 8-member ring of LTA. As can be further observed, $f^*_{rot.}/f_{rot.}$ drops to 8.83×10^{-4} when the molecule approaches windows of LEV framework, and in this case, the rotation of propene molecule around almost all three-axes are constrained (see Supporting Movie S1–S4). Similarly, we also first calculated the critical $f^*_{rot.}/f_{rot.}$ of methane, which is 1.00 in the absence of restriction on rotation. It is 1.59×10^{-1} if rotation around one axis is limited, 2.53×10^{-2} if rotations around two axes are limited, and 4.02×10^{-3} if all three axes are limited. As shown in Figure S6, we simulated $f^*_{rot.}/f_{rot.}$ of methane when approaching the windows of FAU, EUO, LTA, and LEV frameworks. It is found that, as methane molecule passes through 12-member ring of FAU framework, $f^*_{rot.}/f_{rot.}$ is about 9.94×10^{-1}, which is close to 1.0 and indicates that methane molecule can freely rotate around all three axes with negligible limitation. When methane molecule passes through the 10-member ring of EUO framework, $f^*_{rot.}/f_{rot.}$ reduces to 1.57×10^{-1} (close to critical $f^*_{rot.}/f_{rot.}$ of 1.59×10^{-1}) and demonstrates that the rotation around one axis is almost completely restricted. When methane molecule passes through the 8-member ring of LTA framework, $f^*_{rot.}/f_{rot.}$ reduces to 3.95×10^{-2} (close to critical $f^*_{rot.}/f_{rot.}$ of 2.53×10^{-2}) and shows that the rotation around two axes are severely constrained. As can be seen, $f^*_{rot.}/f_{rot.}$ can drop to 6.16×10^{-3} when the molecule approaches windows of LEV framework, and in this case, methane molecule's rotation around almost all three-axes are restricted (see Supporting Movie S5–S8). The MD results discussed above nevertheless can partly support our hypothesis, from a physically meaningful basis, in deriving Equation (4).

For different frameworks, the change of the dimension of cavity and window or pore contractions[32] leads to the decrease in diffusivity, which implies that every molecule in the cavity can have probability g_t to migrate from large cavity to the narrow window by translational motion. In most cases, however, compared to that of rotational partition function, the translational partition function has less pronounced influence on the intracrystalline diffusivity.

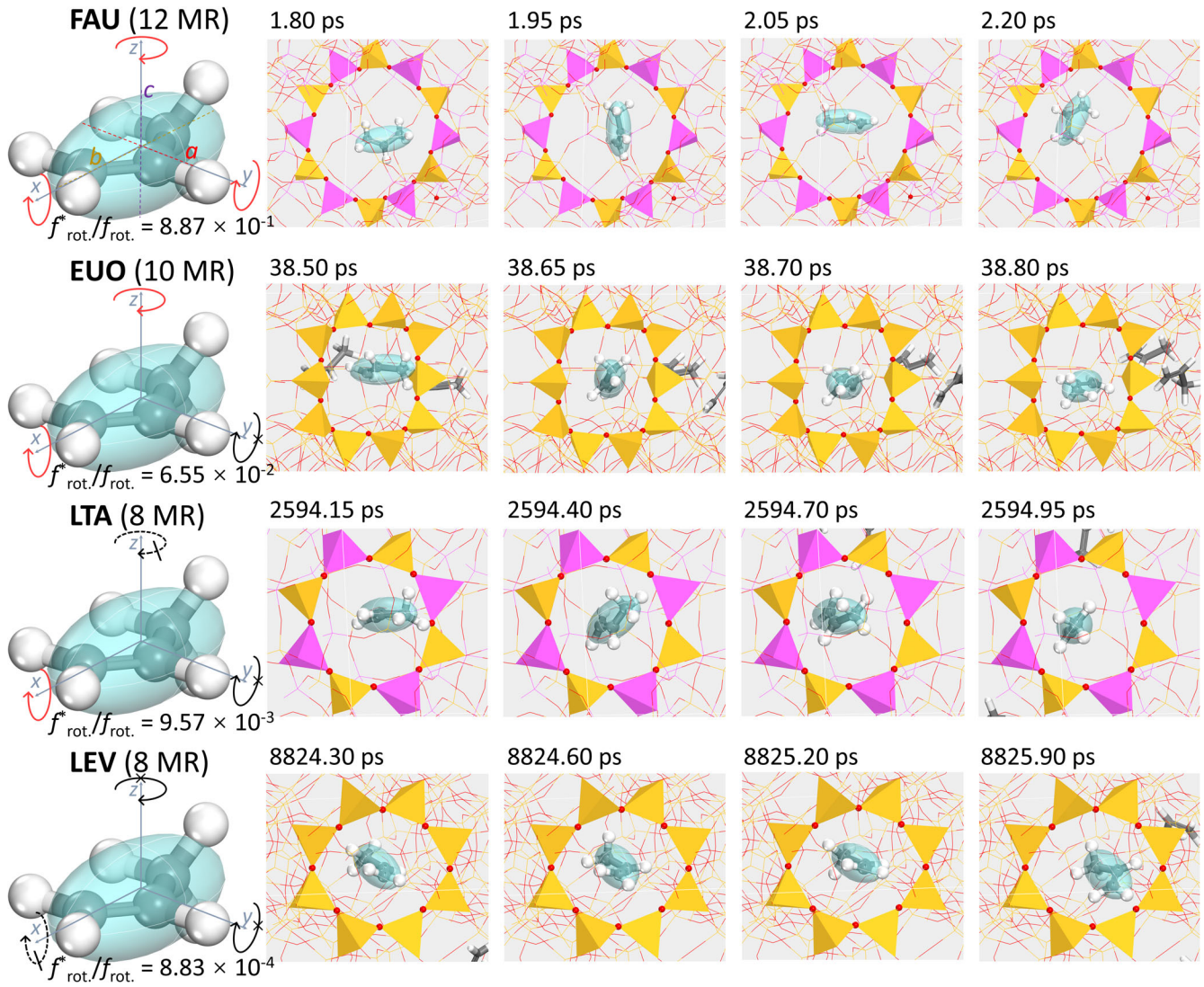

FIGURE 3 Snapshots of propene passing through the windows of different frameworks obtained by MD simulations: FAU (12-member ring), EUO (10-member ring), LTA (8-member ring with window size of 0.415 nm), and LEV (8-member ring with window size of 0.347 nm) (see Supporting Movie S1–S4) [Color figure can be viewed at wileyonlinelibrary.com]

TABLE 2 Parameters A and B_j in FAU, ZSM-5, ZIF-8 MOF, and SAPO-34

Zeolite	d_{cage} (nm)	A_j (–)	B_j (nm^{-1})
FAU	0.729	2.52	3.80
ZSM-5	0.560	2.24	5.80
ZIF-8 MOF	0.410	2.10	11.20
SAPO-34	0.366	2.24	15.50

As can be seen from Figure 2b, the decrease in dimension of window and the increase in molecular diameters can both lead to significant increase in activation energy. Equation (6) has been used to fit the data in Figure 2b for each framework. As can be seen in Table 2 and Figure 2b, for the same framework, B_j reflects the sensitivity of increases in activation energy as the vdW diameter increases. An exponential relationship between B_j and MFSD can be established based on the data for four frameworks (i.e., FAU, MIF, ZIF-8 MOF, and CHA),

$$B_j = (54.90 \pm 2.72)\exp\left(-(3.78 \pm 0.10)d_{\text{window},j}\right) \quad (8)$$

From Figure 2d it can be found that as σ approaches 0.266 nm, which corresponds to the molecules of H_2, the activation energy $E_{a,diff}$ becomes close to 3.40 ± 0.20 kJ/mol. Note that the dimension of windows of these four frameworks are sufficiently larger than the molecular diameters of H_2. For more general situations, an expression that relates the activation energy of diffusion of H_2 to MFSD has been established based on simulation data from a large collection of zeolites and MOFs,[21,35] which reads $E_{a,diff}(H_2) = 9{,}684.10\exp(-29.60d_{window}) + (3.40 \pm 0.20)$ (see Figure S7). Combining this expression with Equation (8), the activation energy of diffusion of a variety of molecules in different frameworks can be obtained through Equation (6).

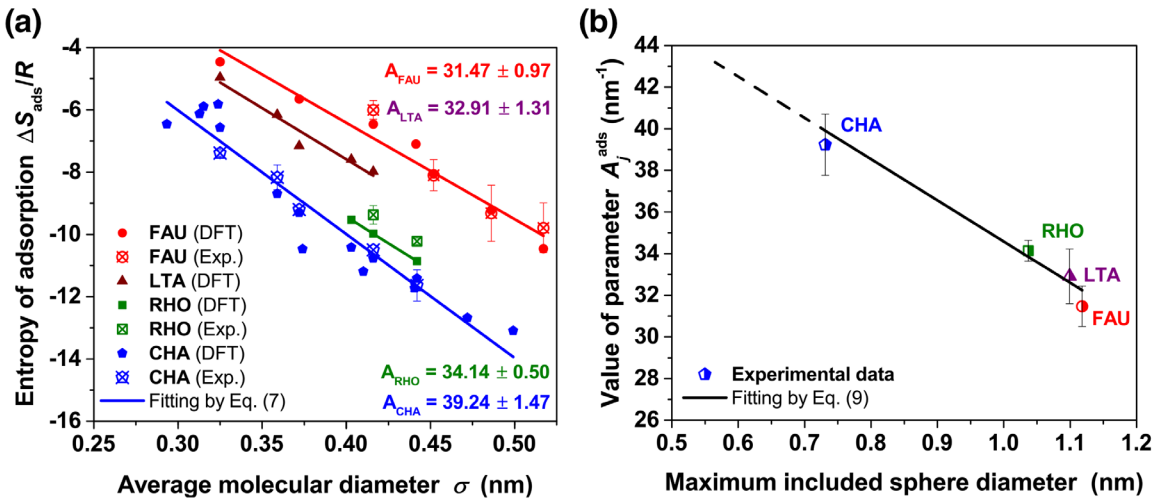

FIGURE 4 (a) Molecular adsorption entropies as function of the average molecular diameter in the H-FAU, Si-LTA, DNL-6 and SAPO-34 zeolites, linear fits by Equation (7). (b) Parameter A_j^{ads} as function of MISD of framework, solid line represents linear fit by Equation (9) [Color figure can be viewed at wileyonlinelibrary.com]

TABLE 3 Parameters A_j^{ads}, $C_{A,j}$, and correlation coefficient R^2 of Equation (7) in H-FAU, Si-LTA, DNL-6, and SAPO-34 zeolites

Zeolite	d_{cage} (nm)	A_j^{ads} (nm^{-1})	$C_{A,j}$ (–)
H-FAU	1.118	30.90	–5.78
Si-LTA	1.099	32.90	–5.57
DNL-6	1.037	35.10	–4.62
SAPO-34	0.731	39.80	–5.84

So far, the translational and rotational partition function of intracrystalline diffusion can be predicted by Equations (3) and (4)/(5), and the activation energy of diffusion $E_{a,diff}$ can be predicted by Equations (6) and (8). Then we can determine the hopping rate k by Equation (2), and further predict the intracrystalline diffusivity by Equation (1).

4.2 | The correlation for adsorption entropy

We studied the adsorption entropies of different molecules for frameworks FAU, LTA, RHO, and CHA, and the results are shown in Figure 4a. As can be seen from Figure 4a, for the same molecule, the loss of adsorption entropy increases in the order H-FAU < Si-LTA < DNL-6 < SAPO-34 (see Section 2 in Supporting Information). This corresponds to the ordering of the adsorption strength: higher entropy loss indicates stronger adsorption due to the confinement of frameworks. Normally smaller cavity leads to a tighter fit of molecules in the frameworks and consequently higher loss in adsorption entropy. This is partly due to the contribution of vdW interaction between molecules and frameworks or the restricted motion of molecules in the confined spaces. Meanwhile for the same framework, increasing molecular diameter of molecules will also result in higher adsorption entropy loss. In fact, as represented by Equation (7), the adsorption entropy can be considered as a linear function of average molecular diameter. However, it should be specified that how to calculate the parameters A_j^{ads} and $C_{A,j}$ used in Equation (7).

Table 3 lists the adsorption entropies for all zeolites studied. As can be found, the adsorption entropy can be fitted by Equation (7) with a coefficient R^2 of 0.9604. In the following, therefore, we further explore the method to calculate A_j^{ads}. From Figure 4a and Table 3, it can be observed that, as the dimension of cavity decreases, A_j^{ads} increases. A_j^{ads} can reflect the sensitivity of the change of adsorption entropy owning to the change of the dimension of cavity for the same guest molecules. For instance, for frameworks with sufficiently small cavity, a minor increase in molecular diameter of molecules would lead to the pronounced adsorption entropy loss, which in turn results in higher A_j^{ads}. Inspired by this, we plotted A_j^{ads} against MISD in Figure 4b. As can be seen, a linear relation also exists between A_j^{ads} and MISD, with a correlation coefficient of R^2 = 0.9302:

$$A_j^{ads} = -(18.51 \pm 0.17) d_{cage,j} + (52.88 \pm 0.21) \quad (9)$$

Based on the data in Table 3, the constant $C_{A,j}$ in Equation (7) can be approximated as −5.44 ± 0.49. Therefore, the adsorption entropy for different frameworks can be predicted via the combination of Equations (7) and (9), suppose that the molecular diameter of the guest molecules is known.

4.3 | Prediction of the intracrystalline diffusivity

We first studied the intracrystalline diffusivity of different guest molecules in nine zeolitic frameworks with varying extents of confinement. These frameworks includes FAU,[2] ISV,[71] MFI,[67,71] ITE,[71,72] LTA,[25,73] IHW,[72] RHO,[74] CHA,[51,52,53,55] and DDR.[2,73] The prediction results

were shown in Figure 5a, in which it shows that the predictions are consistent with results from various simulations and/or experiments. We then studied the effect of confinement on the intracrystalline diffusivity. In doing so, we applied Equations (1) and (2) to predict the diffusivity of methane in 15 zeolitic frameworks. For specified cases where three axes are the same, the ellipsoidal molecules can be simplified to the spherical ones, for example, methane. The predicted intracrystalline diffusivities, as a function of MFSD (i.e., d_{window}), were compared to that derived from MD simulations.[35] As shown in Figure 5b, the predicted results agree well with the MD results with R^2 of 0.9689. In Figure 5b, though both PON and BOF have similar window diameter (d_{window} = 0.424 nm) and hopping distance, d_{cage} of PON (0.487 nm) is about half of d_{cage} of BOF (0.886 nm). According to Equation (3), $g_{trans.}$ is 0.758 for PON and 0.229 for BOF. Approximately, the diffusivity of methane at infinite dilution in PON is five times large than that in BOF.[54] Basically, the increase of MFSD prompts the intracrystalline diffusion of methane in the framework. For MFSD less than 0.6 nm where the confinement of the framework is severe, the contribution of rotational partition function to the diffusivity is prominent as shown in Figure S8. Essentially the rotational partition function reflects that the possibility of suitable orientation of molecules. This is because the narrowing of window may restrict methane molecules to find suitable orientations at which the molecules can cross the narrow window, as shown in Figure S8, which significantly reduces the value of rotational partition function. For MFSD large than 0.6 nm, the slope of intracrystalline diffusivity against MFSD becomes much smaller. This can be explained as that, when the effect of confinement becomes minor, $f^{*}_{rot.}/f_{rot.}$ approach 1.0 as shown in Figure S8 and the intracrystalline diffusivity of methane reaches a relatively narrow range of 10^{-8} ~ 10^{-7} m^2/s. From these discussions, the confinement effect by window on molecular diffusion can be clearly revealed.

To further verify the applicability and accuracy of the proposed methods, Equations (1) and (2) were also applied to predict the

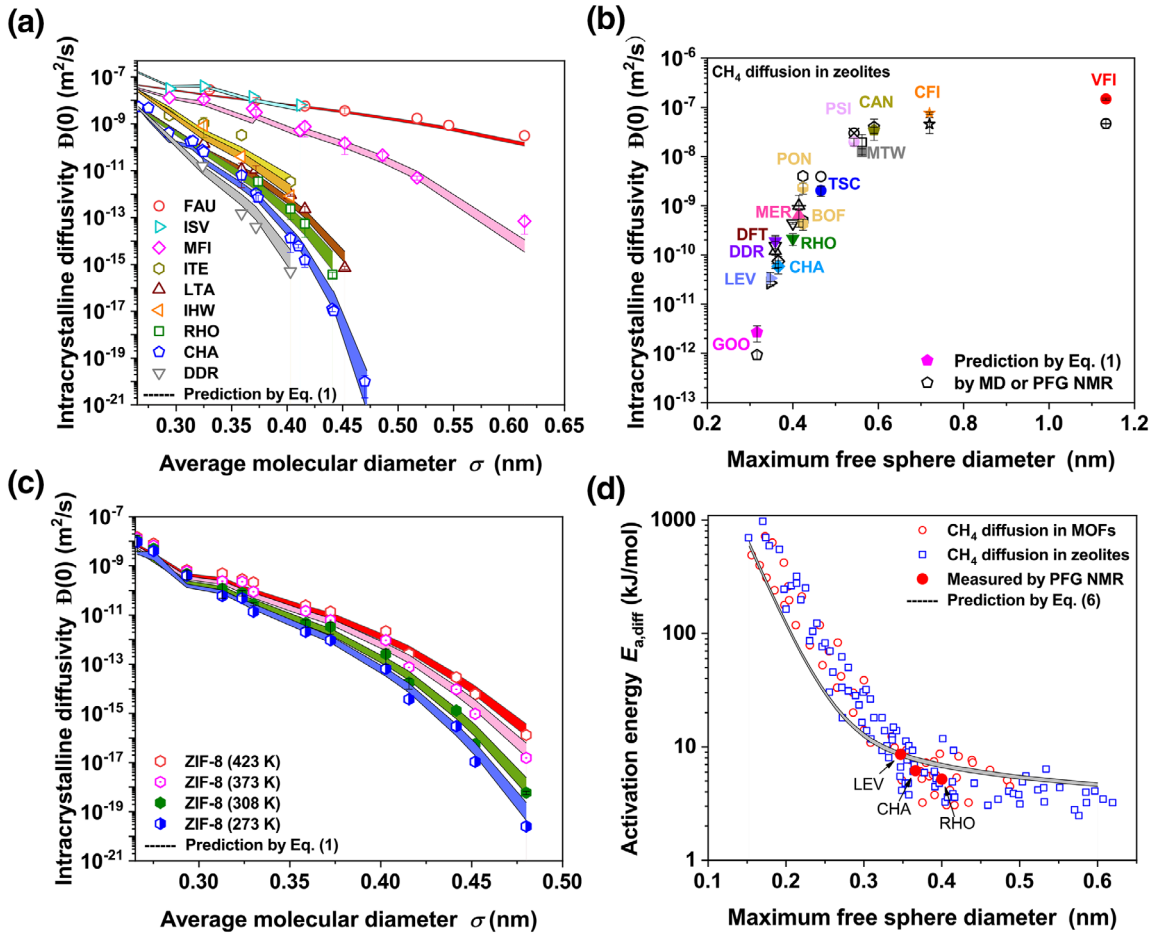

FIGURE 5 (a) Comparisons of predicted and measured intracrystalline diffusivity at infinite dilution for diverse molecules in FAU,[2] ISV,[71] MFI,[67,71] ITE,[71,72] LTA,[25,73] IWH,[72] RHO,[74] CHA,[53,55,63,74] and DDR[2,73] zeolitic frameworks at 300 K. (b) Comparisons of predicted and simulated intracrystalline diffusivity at infinite dilution of methane in VFI, CFI, CAN, MTW, TSC, MER, RHO, CHA, DDR, DFT, LEV, and GOO zeolites[35] at 300 K. (c) Comparisons of predicted and measured intracrystalline diffusivity at infinite dilution for 13 molecules in ZIF-8 MOF at 273, 308, 373, 423 K.[26] (d) Comparisons of predicted and simulated activation energy of diffusion of methane in zeolites[35,74] and MOFs.[21] Intracrystalline diffusivities are predicted by Equation (1) and activation energies are predicted by Equation (6) [Color figure can be viewed at wileyonlinelibrary.com]

diffusion of guest molecules in ZIF-8 MOF under different temperature. The MFSD of ZIF-8 MOF is 0.400 nm.[58] As depicted in Figure 5c, the predicted results can reflect the molecular sieving characteristic of ZIF-8 MOF and are accordance with the simulated intracrystalline diffusivity at 273, 308, 373, 423 K.[26,58] This verifies that activation energies of diffusion predicted by Equations (6) and (8) for diverse molecules are reliable. Then, Equation (6) was extended to calculate the diffusion of methane in a large collection of zeolites and MOFs.[21,35] In Figure 5d, the activation energies of methane predicted by Equations (6) and (8) were compared to the simulation results by MD[21,43] and experimental results by pulsed field gradient (PFG) NMR.[74] In Figure 5d, the predicted activation energies of diffusion are well consistent with experimental results for zeolites.[74] The relative standard deviation from the predictions based on our developed correlations is within 1.29 in Figure 5d. In this work, we mainly considered the effects of confinement of zeolite and MOFs materials on molecular diffusivity. Beyond confinement effects, the interactions between chemical composition of frameworks and molecules, among others, may also play a role in affecting molecular diffusivity in nanoporous crystalline materials.[35,75] The intracrystalline diffusivities at infinite dilution and activation energies of diffusion for 22 frameworks were well predicted by Equations (1) and (6) with a correlation coefficient R^2 of 0.9865. It can be observed that when MFSD increases the activation energy of diffusion of methane demonstrates a remarkable declination. In case of high activation energy of diffusion, even the guest molecules can find suitable orientations to enter window, the strong repulsive potential between molecules and the window would significantly retard the translational motion of molecules.

4.4 | Predictions of the adsorption entropies

In Equation (7), the parameter A_j^{ads} can be determined by Equation (9) with information of MISD of framework, and the parameter $C_{A,j}$ can be treated as a constant contribution of the vdW stabilization. Thus, by use of Equations (7) and (9), the adsorption entropies for various molecules in different frameworks can be predicted, which are shown in Figure 6. The experimental adsorption entropies for various molecules in six zeolitic frameworks, that is, KFI, TON, MFI, FER, MOR, and LTL, which were collected from literature[42,44,45,76] were used for comparison. As shown in Figure 6, the predicted adsorption entropies show good consistence with experimental results for six zeolites, which collapse to a single line. Furthermore, compared to the correlation from reference,[44] the correlation coefficient R^2 has increased from 0.8539 to 0.9154.

4.5 | Applicable scope of correlations

Nanoporous carbon materials are important workhouse in catalysis and gas separation.[32,77,78] Molecular diffusivity in single walled carbon nanotubes (SWNTs) was found to be order of magnitude higher than in zeolites with same window diameter owning to the inherent

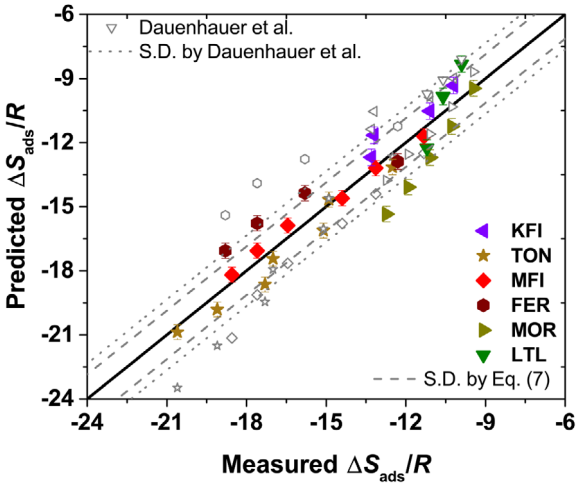

FIGURE 6 Comparisons of predicted and measured adsorption entropies for different molecules in KFI, TON, MFI, FER, MOR, and LTL zeolitic frameworks.[44] Colorful points are predicted by Equation (7) and gray points are predicted from reference[44] [Color figure can be viewed at wileyonlinelibrary.com]

smoothness of SWNTs.[77-79] Essentially, the friction between molecules and wall in SWNTs is much lower than that in zeolite, and such low friction between molecules and wall incurs less frequent molecule-wall collisions and thus reduces momentum loss.[77-79] The correlations proposed in this work were developed mainly for zeolites and MOFs materials. Due to the significant discrepancy of surface roughness between SWNTs and zeolites/MOFs, the correlations were not suitable, at current stage, to predict the diffusivity of molecule in SWNTs. The correlations developed in this work was limited in the diffusion or adsorption of molecule at infinite dilution. The Reed and Ehrlich model[80] can be used to determine the transport diffusivity at different molecular loading based on the diffusivity at low molecular loading Đ(0). Skoulidas and Sholl[71] proposed an empirical relation to link self-diffusivity and transport diffusivity at specific molecular loading. Though the confinement effects imposed by nanocavity or windows of nanoporous crystalline materials have been taken into account, the effect of chemical composition and acidity of framework on diffusivity are mainly caused by complex interaction between framework and molecules.[31,74,75] Different chemical composition and acidity of framework can alter the potential energy of diffusion.[31,75] The effects of chemical composition and acidity of framework need to be further studied with regard to the activation energy of diffusion. Consequently, if may not be feasible to predict molecular diffusivity within zeolites and MOFs materials with strong acidity.[31]

The potential application of proposed correlations is expected to provide fundamental parameters of mass transport and adsorption for heterogeneous catalysis.[1,14,15,18,81] Another application for current correlation is to estimate the ideal separation selectivity for system with low molecular loading or pressure.[21,35] In this case, as shown by Keskin and Sholl,[82] the ideal separation selectivity can be obtained by intracrystalline diffusivity and adsorption entropy suppose the

molecule-molecule interaction is negligible. As for the enthalpy of adsorption, Dauenhauer et al[44] estimated that for every 1 $J \cdot mol^{-1} \cdot K^{-1}$ of adsorption entropy lose there is 509 ± 19 $J \cdot mol^{-1}$ of enthalpy that can be gained,[44] which means that adsorption enthalpy can be predicted from adsorption entropy approximately.

5 | CONCLUSIONS

Quantifying the intracrystalline diffusion and adsorption in confined spaces is a crucial step toward understanding and rational designs of nanoporous crystalline materials. Note that the dimensions of confined spaces are comparable to the diameter of guest molecules in most of nanoporous crystalline materials, the diffusion of molecules in these confined spaces is closely related to the molecular diameter and activation energy barrier. In this work, on the one hand, the diffusion of guest molecules is related to the hopping rate according to the transition state theory, and on the other hand, the hopping rate is further interpreted as a result of combination of contributions by translational and rotational motion. We differentiate and quantify the contribution of translational and rotational motion of guest molecules by use of the partition function, and the interaction between window and guest molecules by use of the repulsive potential. Based on this theoretical analysis, we establish a fundamental approach to quantify the intracrystalline diffusivity and adsorption entropy at infinite dilution based on the partition functions in confining systems. It has been shown that our proposed approach can be used to predict the intracrystalline diffusivity and adsorption entropy for a wide range of frameworks of zeolites and MOFs materials with reasonable accuracy.

It should be stressed that the correlations in this work are restricted to predict the intracrystalline diffusivity and adsorption entropy at infinite dilution in zeolites and MOFs materials. But this is still a very important step as it can favor the understanding the mechanisms underlying the interplay between the confinement effect and intracrystalline diffusion and adsorption, and the establishment the structure–property relationships. Essentially, it can be used as a high-throughput screening tool to identify the ideal materials for gas separation and heterogeneous catalysis in which the diffusion of guest molecules plays a critical role. Finally, it constitutes a potential way for complementing the microkinetic models in zeolitic catalysis such as methanol to hydrocarbons (MTH).

ACKNOWLEDGMENTS

This work is supported by the National Natural Science Foundation of China (Grant No. 91834302). We thank the kind help from Dr Wenna Zhang, Prof Miao Yang, and Dr Pengfei Wu for the theoretical calculation and providing some zeolite samples.

ORCID

Mingbin Gao https://orcid.org/0000-0002-7143-2658
Hua Li https://orcid.org/0000-0003-3291-7844
Mao Ye https://orcid.org/0000-0002-7078-2402

REFERENCES

1. Keil FJ. Molecular modelling for reactor design. *Annu Rev Chem Biomol Eng*. 2018;9:201-227.
2. Kärger J, Ruthven DM, Theodorou DN. *Diffusion in Nanoporous Materials*. Weinheim: Wiley-VCH; 2012.
3. Keil Frerich J, Krishna R, Coppens M-O. Modeling of diffusion in zeolites. *Rev Chem Eng*. 2000;16:71-197.
4. Liu Z, Yi X, Wang G, et al. Roles of 8-ring and 12-ring channels in mordenite for carbonylation reaction: from the perspective of molecular adsorption and diffusion. *J Catal*. 2019;369:335-344.
5. Zhu Z, Wang D, Tian Y, Jiang L. Ion/molecule transportation in nanopores and nanochannels: from critical principles to diverse functions. *J Am Chem Soc*. 2019;141:8658-8669.
6. Sun Z, Wu K, Shi J, et al. Effect of pore geometry on nanoconfined water transport behavior. *AIChE J*. 2019;65:e16613.
7. Liu Y, Guo F, Hu J, Liu H, Hu Y. Molecular transport through mixed matrix membranes: a time-dependent density functional approach. *AIChE J*. 2017;63:4586-4594.
8. Kang JH, Alshafei FH, Zones SI, Davis ME. Cage-defining ring: a molecular sieve structural indicator for light olefin product distribution from the methanol-to-olefins reaction. *ACS Catal*. 2019;9:6012-6019.
9. Baumann AE, Burns DA, Liu B, Thoi VS. Metal-organic framework functionalization and design strategies for advanced electrochemical energy storage devices. *Commun Chem*. 2019;2:86-99.
10. Schwieger W, Machoke AG, Weissenberger T, et al. Hierarchy concepts: classification and preparation strategies for zeolite containing materials with hierarchical porosity. *Chem Soc Rev*. 2016;45:3353-3376.
11. Chmelik C, Kärger J. In situ study on molecular diffusion phenomena in nanoporous catalytic solids. *Chem Soc Rev*. 2010;39:4864-4884.
12. Goetze J, Meirer F, Yarulina I, et al. Insights into the activity and deactivation of the methanol-to-olefins process over different small-pore zeolites as studied with operando UV–vis spectroscopy. *ACS Catal*. 2017;7:4033-4046.
13. Whiting GT, Nikolopoulos N, Nikolopoulos I, Chowdhury AD, Weckhuysen BM. Visualizing pore architecture and molecular transport boundaries in catalyst bodies with fluorescent nanoprobes. *Nat Chem*. 2019;11:23-31.
14. Li H, Ye M, Liu Z. A multi-region model for reaction–diffusion process within a porous catalyst pellet. *Chem Eng Sci*. 2016;147:1-12.
15. Gao M, Li H, Yang M, et al. A modeling study on reaction and diffusion in MTO process over SAPO-34 zeolites. *Chem Eng J*. 2019;377:119668.
16. Ye G, Wang H, Zhou X, Keil FJ, Coppens M-O, Yuan W. Optimizing catalyst pore network structure in the presence of deactivation by coking. *AIChE J*. 2019;65:e16687.
17. Rao SM, Saraçi E, Gläser R, Coppens M-O. Surface barriers as dominant mechanism to transport limitations in hierarchically structured catalysts – application to the zeolite-catalyzed alkylation of benzene with ethylene. *Chem Eng J*. 2017;329:45-55.
18. Hansen N, Krishna R, van Baten JM, Bell AT, Keil FJ. Analysis of diffusion limitation in the alkylation of benzene over H-ZSM-5 by combining quantum chemical calculations, molecular simulations, and a continuum approach. *J Phys Chem C*. 2009;113:235-246.
19. Smit B, Maesen TLM. Towards a molecular understanding of shape selectivity. *Nature*. 2008;451:671-678.
20. Goldsmith BR, Esterhuizen J, Liu J-X, Bartel CJ, Sutton C. Machine learning for heterogeneous catalyst design and discovery. *AIChE J*. 2018;64:2311-2323.
21. Haldoupis E, Nair S, Sholl DS. Efficient calculation of diffusion limitations in metal organic framework materials: a tool for identifying materials for kinetic separations. *J Am Chem Soc*. 2010;132:7528-7539.

22. Fu J, Tian Y, Wu J. Classical density functional theory for methane adsorption in metal–organic framework materials. *AIChE J*. 2015;61:3012-3021.
23. Zhang K, Lively RP, Zhang C, et al. Exploring the framework hydrophobicity and flexibility of ZIF-8: from biofuel recovery to hydrocarbon separations. *J Phys Chem Lett*. 2013;4:3618-3622.
24. Sholl DS. Understanding macroscopic diffusion of adsorbed molecules in crystalline nanoporous materials via atomistic simulations. *Acc Chem Res*. 2006;39:403-411.
25. Boulfelfel SE, Ravikovitch PI, Sholl DS. Modeling diffusion of linear hydrocarbons in silica zeolite LTA using transition path sampling. *J Phys Chem C*. 2015;119:15643-15653.
26. Verploegh RJ, Nair S, Sholl DS. Temperature and loading-dependent diffusion of light hydrocarbons in ZIF-8 as predicted through fully flexible molecular simulations. *J Am Chem Soc*. 2015;137:15760-15771.
27. Bendt S, Dong Y, Keil FJ. Diffusion of water and carbon dioxide and mixtures thereof in mg-MOF-74. *J Phys Chem C*. 2019;123:8212-8220.
28. Liu Z, Chu Y, Tang X, et al. Diffusion dependence of the dual-cycle mechanism for MTO reaction inside ZSM-12 and ZSM-22 zeolites. *J Phys Chem C*. 2017;121:22872-22882.
29. Zimmermann NER, Smit B, Keil FJ. Predicting local transport coefficients at solid–gas interfaces. *J Phys Chem C*. 2012;116:18878-18883.
30. Beerdsen E, Smit B, Dubbeldam D. Molecular simulation of loading dependent slow diffusion in confined systems. *Phys Rev Lett*. 2004;93:248301.
31. Cnudde P, Demuynck R, Vandenbrande S, Waroquier M, Sastre G, Speybroeck VV. Light olefin diffusion during the MTO process on H-SAPO-34: a complex interplay of molecular factors. *J Am Chem Soc*. 2020;142:6007-6017.
32. Bhatia SK. Characterizing structural complexity in disordered carbons: from the slit pore to atomistic models. *Langmuir*. 2017;33:831-847.
33. Nguyen TX, Bhatia SK. Kinetic restriction of simple gases in porous carbons: transition-state theory study. *Langmuir*. 2008;24:146-154.
34. Dutta RC, Bhatia SK. Interfacial engineering of MOF-based mixed matrix membrane through atomistic simulations. *J Phys Chem C*. 2020;124:594-604.
35. Haldoupis E, Nair S, Sholl DS. Pore size analysis of >250 000 hypothetical zeolites. *Phys Chem Chem Phys*. 2011;13:5053-5060.
36. Krishna R. Describing the diffusion of guest molecules inside porous structures. *J Phys Chem C*. 2009;113:19756-19781.
37. Jakobtorweihen S, Keil FJ, Smit B. Temperature and size effects on diffusion in carbon nanotubes. *J Phys Chem B*. 2006;110:16332-16336.
38. Liu Y, Guo F, Hu J, Zhao S, Liu H, Hu Y. Entropy prediction for H_2 adsorption in metal-organic frameworks. *Phys Chem Chem Phys*. 2016;18:23998-24005.
39. Marbach S, Dean DS, Bocquet L. Transport and dispersion across wiggling nanopores. *Nat Phys*. 2018;14:1108-1113.
40. Krishna R, van Baten JM. Unified Maxwell–Stefan description of binary mixture diffusion in micro- and meso-porous materials. *Chem Eng Sci*. 2009;64:3159-3178.
41. Krishna R. Diffusion in porous crystalline materials. *Chem Soc Rev*. 2012;41:3099-3118.
42. De Moor BA, Reyniers M-F, Gobin OC, Lercher JA, Marin GB. Adsorption of C2−C8 n-alkanes in zeolites. *J Phys Chem C*. 2011;115:1204-1219.
43. Nguyen CM, De Moor BA, Reyniers M-F, Marin GB. Physisorption and chemisorption of linear alkenes in zeolites: a combined QM-pot (MP2//B3LYP:GULP)–statistical thermodynamics study. *J Phys Chem C*. 2011;115:23831-23847.
44. Dauenhauer PJ, Abdelrahman OA. A universal descriptor for the entropy of adsorbed molecules in confined spaces. *ACS Cent Sci*. 2018;4:1235-1243.
45. Piccini G, Alessio M, Sauer J, et al. Accurate adsorption thermodynamics of small alkanes in zeolites. Ab initio theory and experiment for H-Chabazite. *J Phys Chem C*. 2015;119:6128-6137.
46. De Moor BA, Ghysels A, Reyniers M-F, Van Speybroeck V, Waroquier M, Marin GB. Normal mode analysis in zeolites: toward an efficient calculation of adsorption entropies. *J Chem Theory Comput*. 2011;7:1090-1101.
47. Denayer JFM, Devriese LI, Couck S, et al. Cage and window effects in the adsorption of n-alkanes on Chabazite and SAPO-34. *J Phys Chem C*. 2008;112:16593-16599.
48. Treacy MMJ, Foster MD. Packing sticky hard spheres into rigid zeolite frameworks. *Microporous Mesoporous Mater*. 2009;118:106-114.
49. Campbell CT, Sellers JRV. The entropies of adsorbed molecules. *J Am Chem Soc*. 2012;134:18109-18115.
50. Zimmermann NER, Balaji SP, Keil FJ. Surface barriers of hydrocarbon transport triggered by ideal zeolite structures. *J Phys Chem C*. 2012;116:3677-3683.
51. Beerdsen E, Dubbeldam D, Smit B. Understanding diffusion in nanoporous materials. *Phys Rev Lett*. 2006;96:044501.
52. Kärger J, Binder T, Chmelik C, et al. Microimaging of transient guest profiles to monitor mass transfer in nanoporous materials. *Nat Mater*. 2014;13:333-343.
53. Dubbeldam D, Snurr RQ. Recent developments in the molecular modeling of diffusion in nanoporous materials. *Mol Simul*. 2007;33:305-325.
54. Liu Z, Zhou J, Tang X, et al. Dependence of zeolite topology on alkane diffusion inside nano-channels. *AIChE J*. 2020;66:e16269.
55. Li S, Falconer JL, Noble RD, Krishna R. Interpreting unary, binary, and ternary mixture permeation across a SAPO-34 membrane with loading-dependent Maxwell−Stefan diffusivities. *J Phys Chem C*. 2007;111:5075-5082.
56. Frisch MJ, Trucks GW, Schlegel HB, et al. *Gaussian 09, Revision B.01*. Wallingford, CT: Gaussian, Inc.; 2016.
57. Lide DR. *CRC Handbook of Chemistry and Physics*. Boca Raton: CRC Press; 2005.
58. Zhang C, Lively RP, Zhang K, Johnson JR, Karvan O, Koros WJ. Unexpected molecular sieving properties of zeolitic imidazolate framework-8. *J Phys Chem Lett*. 2012;3:2130-2134.
59. London F. The general theory of molecular forces. *Trans Faraday Soc*. 1937;33:8-26.
60. DÜRen T, Keil FJ, Seaton NA. Molecular simulation of adsorption and transport diffusion of model fluids in carbon nanotubes. *Mol Phys*. 2002;100:3741-3751.
61. Skoulidas AI, Sholl DS. Transport diffusivities of CH_4, CF_4, He, Ne, Ar, Xe, and SF6 in silicalite from atomistic simulations. *J Phys Chem B*. 2002;106:5058-5067.
62. Foster MD, Rivin I, Treacy MMJ, Delgado Friedrichs O. A geometric solution to the largest-free-sphere problem in zeolite frameworks. *Microporous Mesoporous Mater*. 2006;90:32-38.
63. Gao M, Li H, Yang M, et al. Direct quantification of surface barriers for mass transfer in nanoporous crystalline materials. *Commun Chem*. 2019;2:43-52.
64. Wu P, Yang M, Zhang W, et al. Silicoaluminophosphate molecular sieve DNL-6: synthesis with a novel template, N,N′-dimethylethylenediamine, and its catalytic application. *Chin J Catal*. 2018;39:1511-1519.
65. *Database of Zeolite Structures*. http://www.iza-structure.org/databases/.
66. Zhang W, Chen J, Xu S, et al. Methanol to olefins reaction over cavity-type zeolite: cavity controls the critical intermediates and product selectivity. *ACS Catal*. 2018;8:10950-10963.
67. Datema KP, den Ouden CJJ, Ylstra WD, Kuipers HPCE, Post MFM, Kärger J. Fourier-transform pulsed-field-gradient 1H nuclear magnetic resonance investigation of the diffusion of light

n-alkanes in zeolite ZSM-5. *J Chem Soc Faraday Trans*. 1991;87:1935-1943.
68. Remy T, Cousin Saint Remi J, Singh R, Webley PA, Baron GV, Denayer JFM. Adsorption and separation of C1–C8 alcohols on SAPO-34. *J Phys Chem C*. 2011;115:8117-8125.
69. Cousin Saint Remi J, Baron GV, Denayer JFM. Nonuniform chain-length-dependent diffusion of short 1-alcohols in SAPO-34 in liquid phase. *J Phys Chem C*. 2013;117:9758-9765.
70. Bonilla MR, Valiullin R, Kärger J, Bhatia SK. Understanding adsorption and transport of light gases in hierarchical materials using molecular simulation and effective medium theory. *J Phys Chem C*. 2014;118:14355-14370.
71. Skoulidas AI, Sholl DS. Molecular dynamics simulations of self-diffusivities, corrected diffusivities, and transport diffusivities of light gases in four silica zeolites to assess influences of pore shape and connectivity. *J Phys Chem A*. 2003;107:10132-10141.
72. Combariza AF, Sastre G, Corma A. Molecular dynamics simulations of the diffusion of small chain hydrocarbons in 8-ring zeolites. *J Phys Chem C*. 2011;115:875-884.
73. Hedin N, DeMartin GJ, Roth WJ, Strohmaier KG, Reyes SC. PFG NMR self-diffusion of small hydrocarbons in high silica DDR, CHA and LTA structures. *Microporous Mesoporous Mater*. 2008;109:327-334.
74. Gao S, Liu Z, Xu S, et al. Cavity-controlled diffusion in 8-membered ring molecular sieve catalysts for shape selective strategy. *J Catal*. 2019;377:51-62.
75. Ghysels A, Moors SLC, Hemelsoet K, et al. Shape-selective diffusion of olefins in 8-ring solid acid microporous zeolites. *J Phys Chem C*. 2015;119:23721-23734.
76. De Moor BA, Reyniers M-F, Marin GB. Physisorption and chemisorption of alkanes and alkenes in H-FAU: a combined ab initio–statistical thermodynamics study. *Phys Chem Chem Phys*. 2009;11:2939-2958.
77. Skoulidas AI, Ackerman DM, Johnson JK, Sholl DS. Rapid transport of gases in carbon nanotubes. *Phys Rev Lett*. 2002;89:185901.
78. Chen H, Sholl DS. Rapid diffusion of CH_4/H_2 mixtures in single-walled carbon nanotubes. *J Am Chem Soc*. 2004;126:7778-7779.
79. Bhatia SK, Chen H, Sholl DS. Comparisons of diffusive and viscous contributions to transport coefficients of light gases in single-walled carbon nanotubes. *Mol Simul*. 2005;31:643-649.
80. Reed DA, Ehrlich G. Surface diffusion, atomic jump rates and thermodynamics. *Surf Sci*. 1981;102:588-609.
81. Keil FJ. Diffusion and reaction in porous networks. *Catal Today*. 1999;53:245-258.
82. Keskin S, Sholl DS. Efficient methods for screening of metal organic framework membranes for gas separations using atomically detailed models. *Langmuir*. 2009;25:11786-11795.

SUPPORTING INFORMATION

Additional supporting information may be found online in the Supporting Information section at the end of this article.

How to cite this article: Gao M, Li H, Ye M, Liu Z. An approach for predicting intracrystalline diffusivities and adsorption entropies in nanoporous crystalline materials. *AIChE J*. 2020;66:e16991. https://doi.org/10.1002/aic.16991